JOURNAL OF MATERIALS SCIENCE 25 (1990) 5125–5133

Crack-tip damaged zones in rubber-toughened amorphous polymers: a micromechanical model

O. MAUZAC, R. SCHIRRER
Institut Charles Sadron (CRM-EAHP), 4 rue Boussingault, F-67000 Strasbourg, France

The various stages of crack propagation in rubber-toughened amorphous polymers (onset and arrest, stable and unstable growth) are governed by the rate of energy dissipation in the crack-tip damaged zone; hence the relationship between the applied stress intensity factor K_I and the damaged zone size is of utmost importance. The size of the crack-tip damaged zone has been related to K_I via a parameter which is characteristic of the material in given conditions: this factor is proportional to the threshold stress for damage initiation in a triaxial stress field, and has been denoted by σ^*. Theoretical values of σ^* have been calculated by means of a micromechanical model involving the derivation of the stresses near the particles and the application of damage initiation criteria. The morphology, average size and volume fraction of the rubbery particles have been taken into account together with the nature of the matrix. The calculated values of σ^* have been successfully compared with the experimental ones, for a wide set of high-impact polystyrenes (HIPS) and rubber-toughened poly(methyl methacrylate) (RTPMMA).

Nomenclature

PS; HIPS: polystyrene; high-impact polystyrene
PMMA; RTPMMA: poly(methyl methacrylate); rubber-toughened PMMA
MI; CS/H; CS/R: particle morphologies ("multiple inclusion"; "hard core – rubber shell"; "rubber core – rigid shell")
K_r; K_g: bulk moduli of rubber and glassy materials
G_r; G_g: shear moduli of the same materials
v_p: particle volume fraction
L: mean centre-to-centre distance between neighbouring particles
B; H; W: standard names for the dimensions of the compact tension specimen
R_y: size of the crack-tip plastic zone in a homogeneous material
h: half thickness of the crack-tip damaged zone
r; θ: polar coordinates around the crack tip (Fig. 1)
r; r_p: distance from particle centre; particle radius
ρ: normalized distance from the particle (Equation 5)
K_I; K_{Ic}; K_{Ip}: stress intensity factor; critical values of K_I at the onset of and during crack growth
G_{Ic}: plane strain energy release rate
σ_y: yield stress in uniaxial tension
σ_{th}: macroscopic threshold stress for the onset of local damage initiation in a composite material
σ^*: characteristic parameter (Equation 3)
$\boldsymbol{\sigma}^0$; σ_1^0; σ_2^0; σ_3^0: applied stress tensor and its three principal stresses
σ^0: uniaxial applied stress
$\boldsymbol{\sigma}$; σ_1; σ_2; σ_3: local stress tensor and its three principal stresses
A: tensor which elements are the ratios of those of $\boldsymbol{\sigma}$ over those of $\boldsymbol{\sigma}^0$ (Equation 4)
v: Poisson's coefficient of the matrix
g: triaxiality factor of the crack-tip stress field
σ_e; σ_p: Mises equivalent stress; dilatational stress (negative pressure)
I_1; I_2: invariants of the stress tensor
U_1; U_2: material parameters for argon and Hannoosh's craze initiation criterion (Equation 12)

1. Introduction

One of the main improvements provided to the mechanical properties of polymers by the introduction of a dispersed rubbery phase is that cracks do not usually propagate as easily as in the parent polymer, thus catastrophic brittle failures are avoided. Many reviews [1, 2] and specialized papers [3–6] addressing this question have been published already, and it is now well established that the origin of toughness lies in the large number of crazes and shear bands initiated at the rubbery particles. More precisely, toughness is qualitatively related to the presence of a damaged ("whitened") zone around the crack tip, and quantitatively to the amount of damaged material inside it [7, 8]. In fact, even brittle failure in homogeneous glassy polymers involves the propagation of a small plastic zone controlling the energy release rate G_{IC} and is, from a microscopical point of view, a ductile failure too.

The theory relating the micromechanisms involved in crack propagation with toughness still has to be achieved for the case of rubber-toughened polymers. As a matter of fact, crack propagation in tough polymers is usually studied from a rather phenomenological point of view [9–11], whereas the more fundamental topic of the micromechanisms of failure is studied in the case of unnotched specimens [12–17].

0022–2461/90 $03.00 + .12

Guild and Young [18] analysed the case of hard particles in epoxy matrix subjected to a uniaxial stress, and drew some conclusions about crack propagation.

In this paper, triaxial states of stress (and the crack-tip stress field in particular) will be considered. It will be shown that a further development of some existing models allows the prediction of the size of the crack-tip damaged zone in heterogeneous materials, provided their structure is known. This is a first step towards quantitative relationships between material's structure, experimental conditions, and fracture toughness of cracked specimens. Theoretical predictions have been compared with experimental data obtained on various high-impact polystyrene (HIPS) and rubber-toughened poly(methyl methacrylate) (RTPMMA).

2. Characterization of the size of the damaged zone

2.1. Choice of a characteristic parameter

The size of the damaged zone increases with increasing stress intensity factor K_I, at least until the crack starts to propagate.

Stresses are partly relieved inside the damaged zone, thus the onset of crack propagation occurs at a higher value of K_I than in the untoughened material (propagation starts when the fibrils at the back of the crack-tip craze break, which occurs under a characteristic craze stress [19]). During crack growth, additional blunting often takes place via the initiation of bunches of short cracks and crazes. Both these facts should be taken into account for calculating critical values of K_I at the onset of (K_{Ic}) or during (K_{Ip}) crack propagation. However, the first problem to treat consists of finding experimental and theoretical means for deriving the material characteristic parameter relating the size of the damaged zone to the applied K_I. The knowledge of this parameter presents further and perhaps more important interests, since it allows the prediction of the volume of the zone where energy-consuming processes occur.

This parameter is proportional to the yield stress in the case of the plastic zone in a homogeneous polymer [20]:

$$R_y \sim (K_I/\sigma_y)^2 \quad (1)$$

where R_y is the size of the plastic zone and σ_y is the yield stress.

In heterogeneous materials however the term "damaged zone" is more accurate than "plastic zone"; likewise "damage initiation threshold stress" (σ_{th}) for example should be used instead of "yield stress". The damage initiation threshold can be represented by a surface in the three-dimensional space of principal stresses, thus σ_{th} is a function of the location around the crack tip. The corresponding relation writes:

$$r(\theta) \sim [K_I/\sigma_{th}(\theta)]^2 \quad (2)$$

where θ is the angular coordinate in the plane normal to the specimen thickness and $r(\theta)$ is the border of the damaged zone (Fig. 1).

The threshold stress for damage initiation σ_{th} is precisely what the theories quoted above [12–17] predict. There are two advantages in deriving this stress through measurements of damaged zone size, rather than through direct measurement in tension or combined tension and torsion on unnotched specimens: (1) experimental results are not affected by the surface quality of the specimen (surface crazing), (2) the measurement of the profile $r(\theta)$ of the damaged zone yields not only a single value of σ_{th} in a given state of (usually uniaxial) stress, but a large part of the critical surface that represents the damage initiation criterion in the space of positive principal stresses.

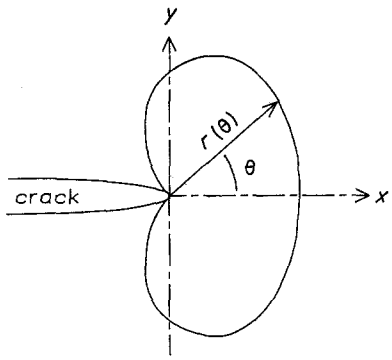

Figure 1 Schematic profile of a damaged zone at a crack tip.

Unfortunately an accurate measurement of the profile cannot be easily made during the growth of the damaged zone, mainly because of the curvature of the crack tip through the specimen thickness. Any uncertainty on the position of the crack tip yields large errors on the values of σ_{th}; the simplest way to avoid such problems is to measure the thickness $2h$ of the damaged zone (Fig. 2). The corresponding parameter, σ^*, is defined by the following relation:

$$h = (K_I/\sigma^*)^2 \quad (3)$$

h is the largest projection of $r(\theta)$ on the vertical axis in Figs 1 and 2; σ^* is not equal, but proportional to the damage initiation threshold stress.

Finally it should be noticed that σ^* and σ_{th} are critical stresses related to local damage initiation in a heterogeneous material, as opposed to the macroscopic yield stress. If σ_{th} is applied to the composite material, damage initiation occurs at the particles, where the local level of stress is enhanced; however, if the particle volume fraction is low enough, the material may not be yielding at the macroscopic scale.

2.2. Experimental details

2.2.1. Materials

Commercial and prototype HIPS and RTPMMA were used in this study. Some of them (HIPS S3-S6) have been supplied by Professor C. B. Bucknall and Dr I. K. Partridge, who have used them previously [21]. The rubbery particles in the materials belong to two main groups: mass polymerized "salami" or "multiple inclusions" (MI) particles, and emulsion polymerized, "core-shell" particles. "Core-shell, hard core" (CS/H) particles consist of a rubbery shell around a rigid core, with an outer shell made of the same material as the matrix in order to ensure adhesion. "Core-shell, rubbery core" (CS/R) particles simply consist of an outer shell (for adhesion too) around a rubbery core.

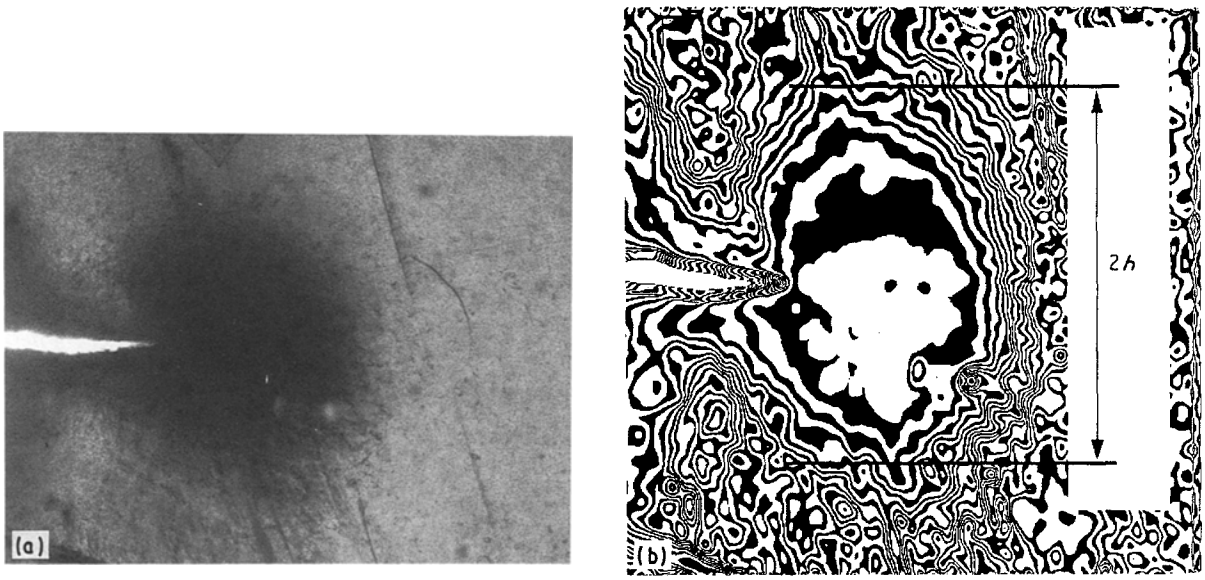

Figure 2 Image analysis of the shadow photograph of a damaged zone. (a) original photograph (linear palette); (b) lines of equal transmitted light amplitude (loop-hole palette).

The materials and their compositions are listed in Table I. The particle size r_p and the particle volume fraction v_p do not include the outer glassy shell when it exists. The particle size indicated is the number average radius; as a general rule the distribution of sizes is broad for MI particles and much narrower for CS ones.

2.2.2. Procedure

Compact tension specimens (width $W = 30$ mm, height $2H = 36$ mm) were cut from compression moulded plates of various thicknesses ($B = 6$ to 20 mm). A thin crack was introduced by 20 Hz fatigue loading (for RTPMMA) or by razor notching (for HIPS). The specimens were tested on a hydraulic Instron 8031 tensile machine operating at a constant, low crosshead speed (0.01 to 0.2 mm sec^{-1}).

The fact that all materials were transparent (RTPMMA) or at least translucent (HIPS) allowed the highly diffusing damaged zone to be observed in transmitted light. Shadow photographs of the crack tip region were taken during the experiments, and the load against displacement curves were recorded. The crack length was measured on each photograph, thus precise values of K_I could be calculated. Image analysis of the photographs also yielded the optical density profile of the damaged zone (Fig. 2); the width $2h$ of the zone was taken at the maximum gradient of optical density in order to avoid plane stress border effects and other surface effects (Fig. 3).

TABLE I Description of the materials used in the experiments

Name	Matrix	v_p (%)	Particles		
			r_p (μm)	Morphology	% Rubber in particle
S1	PS	24	5	MI	30
S2	PS	11	1.5	MI	15
S3 (*:E)	PS	17	0.8	MI	24
S4 (*:A)	PS	17	0.2	MI	39
S5 (*:C)	PS	17	0.1	CS/H	50
S6 (*:D)	PS	17	0.2	CS/H	31
M1	PMMA	30	0.15	CS/H	30
M2	PMMA	36	0.1	CS/H	30
M3	PMMA	25	0.1	CS/H	30
M4	PMMA	30	0.1	CS/R	100

(*): these materials had been previously studied by C. B. Bucknall *et al.* [21]; letters are their names in that paper.

2.2.3. Results

In agreement with Equation 3, it was found that h is proportional to K_I^2. Experimental values of σ^* are reported in Table II . For HIPS they fall in the range 40 to 70 MPa, whereas those for RTPMMA are above 100 MPa, which means that damaged zones at given K_I are much smaller in the latter materials. Some influence of the deformation rate (taken as the slope of the linear part of the curve K_I against time) has been noticed.

3. Theoretical model

Oxborough and Bowden [14], Argon and Boyce [12, 13] and Ricco *et al.* [15] all calculated the stresses in the matrix near the particles, where they are the highest, and then applied some damage initiation criteria. A similar procedure has been applied here. Indeed, most of the parameters used in the following calculations were obtained from the literature; the point where the work reported here is different is that

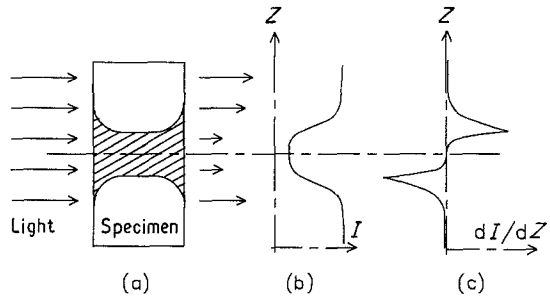

Figure 3 (a) Variation of the size of the damaged zone through the specimen thickness; (b) amplitude of light transmitted through the specimen; (c) gradient of the amplitude of transmitted light.

it deals with a case where stress fields are triaxial even in a homogeneous material. Among the references quoted above, only Oxborough and Bowden considered a combination of a tensile and a compressive stresses applied to a particle, whereas in this report all three principal applied stresses are positive. In such a stress field with a positive dilatational component, the initiation of crazes at particles is more likely than that of shear bands, as verified by Bucknall and Marchetti [6]. Consequently it was assumed in the calculations that damages consisted of crazes; however, the case of shear bands could be easily treated in a similar way.

The theoretical profile $r(\theta)$ of the crack-tip damaged zone at given K_I was calculated, which enabled σ^* to be obtained.

3.1. Stresses around the particles

3.1.1. Isolated particle in a uniaxial stress field

In the case of a uniaxial stress σ^0 applied to an isolated particle, stresses are triaxial at any place in the vicinity of the particle. Stress concentration is maximum at the particle/matrix interface and decreases quickly with distance from the particle. An analytical solution was given by Goodier [22] for a homogeneous spherical particle; data for a wider set of particle morphologies were calculated by Boyce and Argon [12, 13]. Considering that the applied stress defines the polar axis of the particle, the highest principal stresses are situated at the poles and along the equator. At these places two of the principal stresses are tangent to the interface, and the third one is normal to it (Fig. 4).

The perturbation of the applied stress field is expressed as a set of ratios of the local principal stresses σ_i to σ^0:

$$A_i = \sigma_i/\sigma^0 \quad (4)$$

In Fig. 5 the A_i calculated by Boyce for three typical particle morphologies are plotted against the normalized distance from the particle/matrix interface, ρ,

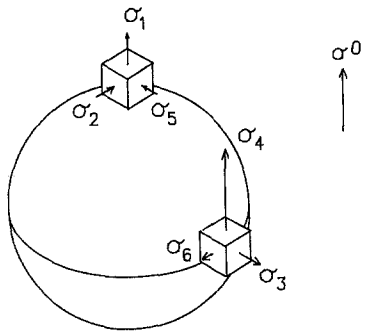

Figure 4 Uniaxial applied stress σ^0, and local triaxial stress fields near a pole (σ_1, σ_2, σ_5) and the equator (σ_3, σ_4, σ_6) of a particle.

as defined by the following equation:

$$\rho = (r - r_p)/r_p \quad (5)$$

where r_p is the particle radius and r is the distance from the centre of an isolated particle.

These model morphologies shall be used throughout this paper.

1. "MI" is a spherical composite particle containing 85% volume of rigid occlusions of various sizes (discontinuous dispersed phase) in a continuous rubber phase.
2. "CS/H" consists of a spherical rigid core surrounded by a rubber shell and a rigid outer shell ensuring a good adhesion with the matrix. The rubber volume fraction inside the particle is 33% (the rigid outer shell being considered as belonging to the matrix).
3. "CS/R" is a pure rubber particle (with a rigid shell for adhesion too).

It is assumed that the adhesion between particle and matrix is perfect.

In her calculations Boyce used the following values for the bulk (compression) and shear moduli K and G, respectively for rubber (index r) and glassy polymer

TABLE II Comparison of the theoretical and experimental values of σ^*

Material name	Experiments				Theory
	t (°C)	Rate (MPa m$^{1/2}$ sec^{-1})	K_{Ic} (MPa m$^{1/2}$)	σ^*_{exp} (MPa)	σ^*_{th} (MPa)
S1	24	0.006	$\simeq$0.9	50.2	50.7
		0.008	$\simeq$1.1	52.0	50.7
S2	22	0.012	unknown	$\simeq$66	52.5
S3	25	0.008	$\simeq$1.4	46	53.1
		0.025	$\simeq$1.6	49	53.1
S4	25	0.08	$\simeq$1.7	$\simeq$69	54.5
S5	25	0.004	$\simeq$1.9	42	48
		0.004	$\simeq$2.0	$\simeq$59	48
S6	25	0.006	$\simeq$1.7	50	47
M1	20	0.02	1.6	136	128
		0.05	1.9	137	128
M2	20	0.002	2.1	125	122
M3	20	0.002	1.7	134	135
M4	20	0.04	1.3	100	115
		0.1	1.4	115	115

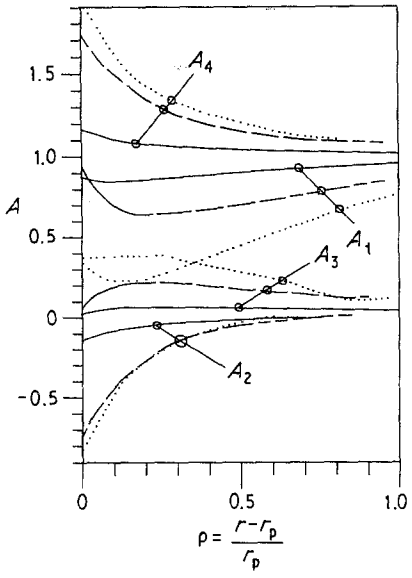

Figure 5 Local stresses near the pole and the equator of an isolated particle of radius r_p, plotted in units of the uniaxial applied stress, against the normalized distance from the particle. (——) MI particle; (– – –) CS/H particle; (· · · ·) CS/R particle. ($A_6 \simeq 0$ and $A_5 = A_2$).

(PS or PMMA, index g):

$$K_r = 1900\,\text{MPa} \quad G_r = 0.6\,\text{MPa}$$

$$K_g = 3200\,\text{MPa} \quad G_g = 1250\,\text{MPa}$$

3.1.2. Particle size effect

It has been reported by Donald and Kramer [5] that craze initiation at a particle requires that the enhanced stress field acts on a large enough distance from the particle, in order that a few craze fibrils can be formed. He evaluated this critical length to be 75 nm. From this point of view, particle size is an important parameter, especially with small particles (less than 1 μm): Goodier's expressions and Boyce's results indicate that the stress enhancements in the matrix roughly decrease by $(r_p/r)^3$, where r_p is the particle radius and r is the distance from the centre of the particle. Consequently, when dealing with craze initiation it was chosen to consider the less favourable of the states of stress that existed from the particle/matrix interface up to a distance of 75 nm (in all cases the maxima of principal stresses occurred at the interface, even for the highest particle volume fractions).

3.1.3. Particle volume fraction effect

When the particle volume fraction is above about 10%, stress perturbations overlap. There are only a limited amount of data available on this effect [12, 13, 16], thus corrections to the local stresses σ_i had to be calculated.

Since calculations consider statistical mean values of interactions between many particles, inhomogeneities in particles distribution have not been taken into account. It has been assumed also that all the particles are spherical and have the same size. The relationship between the average centre-to-centre interparticle distance L and the particle volume fraction v_p is given by:

$$v_p = (4\pi/3)(r_p/L)^3 \qquad (6)$$

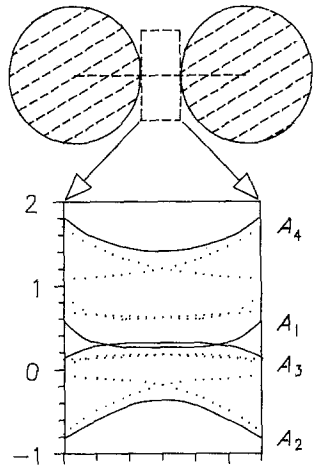

Figure 6 Addition of the stress perturbations between two neighbouring particles. A_1 and A_2 correspond to the case of an external stress applied along the horizontal axis of the figure, A_3 and A_4 to an external stress applied along the vertical axis.

The perturbation of the stress field is obtained by subtracting the global applied stress tensor (σ^0) from the local one (σ): in the case of the uniaxial applied stress σ^0 its normalized components are $A_1 - 1$, A_2, A_3 and $A_4 - 1$ ($A_5 = A_2$ and $A_6 \simeq 0$). It has been considered that between two neighbouring particles the perturbations due to the two particles were additive (Fig. 6). This linear model slightly underestimates the true pertubations of the stresses which would be better calculated using a finite element method (especially for particle volume fractions above 30% [16]). However, in the present case where the bulk moduli of the matrix and the particles are not very different, this model is a good approximation, in particular it is more realistic than Ishai and Cohen's one [23], which considers that the inclusions do not bear any load and yields high upper bounds for A_4:

$$A_{4(\text{I.C.})} = 1/[1 - \pi(r_p/L)^2]$$

$$\simeq 1/(1 - 1.21 v_p^{2/3}) \qquad (7)$$

Fig. 7 gives the corrected local stress factors A_i for the three particle morphologies and for various particle volume fractions, as a function of the normalized distance ρ from the interface.

3.1.4. Crack-tip multiaxial stress field

Dealing with the growth of the damaged zone means describing the displacement of the border behind which damages have been initiated in the material: thus, outside of the damaged zone the assumptions of linear elasticity are still valid and the principle of superposition of stresses can be used. In the case of the triaxial applied stress field, local stress fields were calculated by summing the three tensors corresponding to the individual contributions of the principal applied stresses.

The principal applied stresses σ_1^0, σ_2^0 and σ_3^0 define six poles P_1 and P_1', P_2 and P_2', P_3 and P_3' (Fig. 8), where the maxima of the modified stresses are situated and where both the applied and modified stress tensors (σ^0 and σ) have the same eigen directions. If (i, j, k) is an even permutation of the indexes (1, 2, 3), the principal

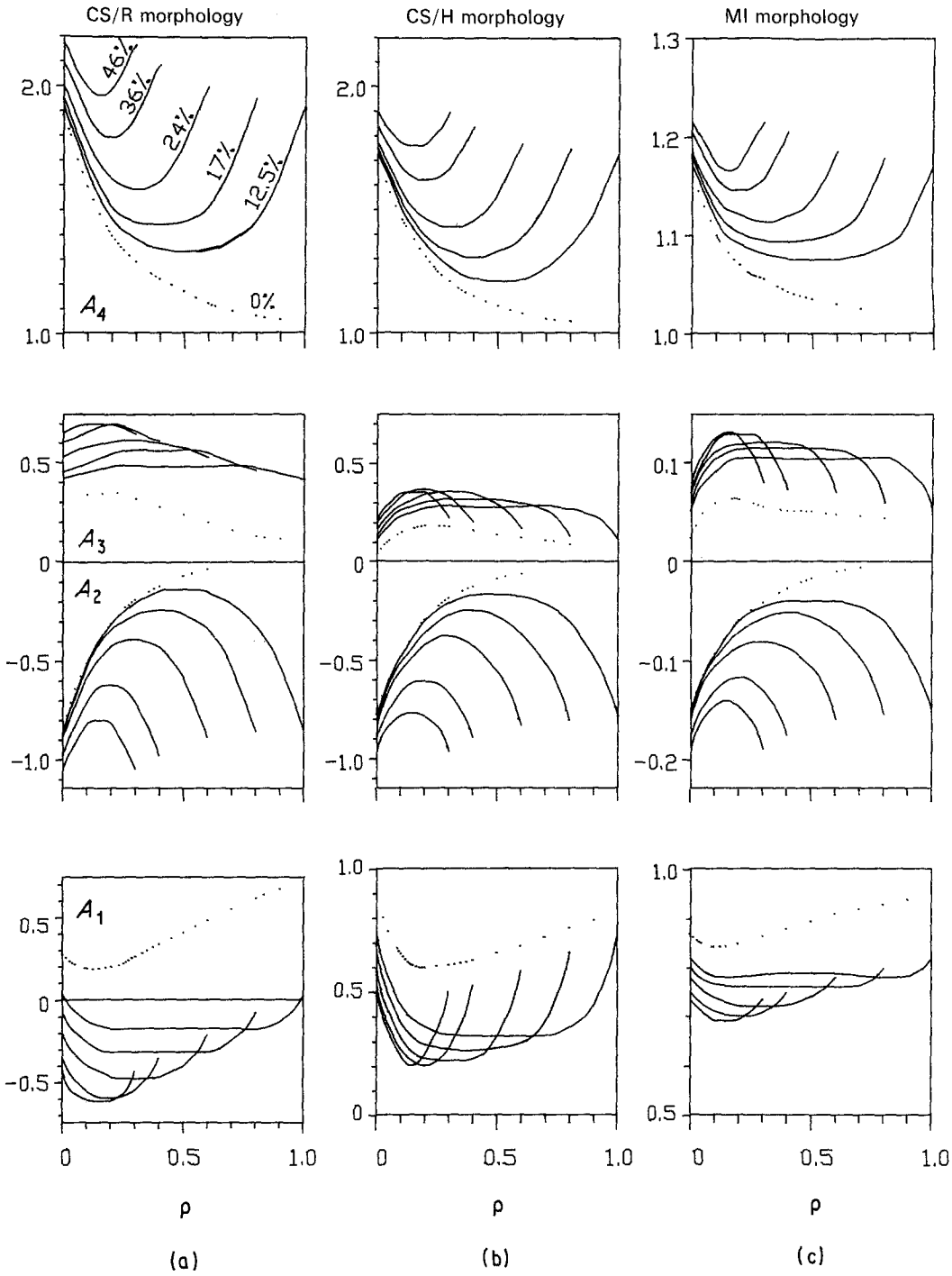

Figure 7 Local stress factors A_i (see text and Figs 4 to 6) for the three particle morphologies and for various particle volume fractions: (a) CS/R; (b) CS/H; (c) MI. The length of the horizontal axis corresponds to one particle radius: for each particle volume fraction the factors A_i have been plotted along a length equal to the mean border-to-border interparticle distance.

modified stresses at the pole i are expressed as:

$$\left\{\begin{array}{rcl}\sigma_i &=& A_1 \cdot \sigma_i^0 + A_3 \cdot (\sigma_j^0 + \sigma_k^0) \\ \sigma_j &=& A_2 \cdot \sigma_i^0 + A_4 \cdot \sigma_j^0 + A_6 \cdot \sigma_k^0 \\ \sigma_k &=& A_2 \cdot \sigma_1^0 + A_6 \cdot \sigma_j^0 + A_4 \cdot \sigma_k^0\end{array}\right\} \quad (8)$$

The applied stress field, written in principal stresses, is [24]:

$$\boldsymbol{\sigma}^0(r, \theta) = \{[K_1 \cdot \cos(\theta/2)]/(2\pi r)^{1/2}\} \times \begin{bmatrix} 1 - \sin(\theta/2) & 0 & 0 \\ 0 & 1 + \sin(\theta/2) & 0 \\ 0 & 0 & 2g \cdot \nu \end{bmatrix} \quad (9)$$

K_1 is the stress intensity factor, ν is Poisson's coefficient of the matrix and g is a triaxiality factor ($g = 0$ in plane stress and $g = 1$ in plane strain); r and θ are the polar coordinates around the crack tip (Fig. 1).

This expression is valid outside of the damaged zone, as long as r is less than 10 mm for the specimen size and geometry that were used (to avoid border effects).

3.1.5. Thermal shrinkage stresses

The effects of the thermal residual stresses were first taken into account. These stresses arise from the different contractions of rubber and glassy materials during the cooling stage after the material has been

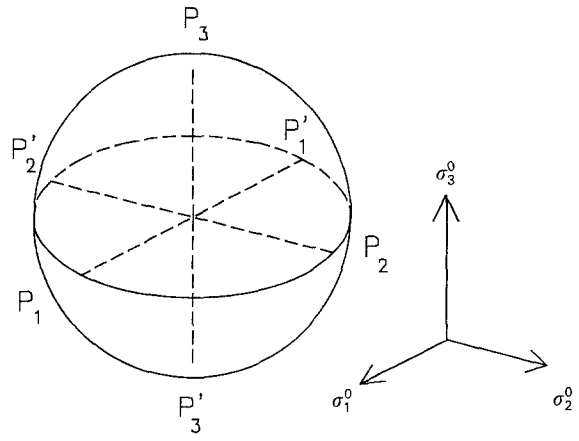

Figure 8 Triaxial applied stress field with the directions of its principal stresses σ_1^0, σ_2^0, σ_3^0 defining six "poles" on the particle.

processed. In the case of particles containing high proportions of glassy material, these stresses are moderate and their influence can be neglected. Conversely, in the case where few or no glassy occlusions exist, the calculated stresses are so high that many crazes should be quickly initiated even in the absence of any applied stress. Indeed this is what happens in some model HIPS; in commercial grades, however, the presence of plasticiser and the breadth of the distribution of molecular masses ensure that most of these stresses are relaxed. Additionally, the rubber in the so-called "pure rubber particles" (CS/R) and in the CS/H ones is usually blended with about 13% polystyrene in order to match the optical index of the matrix (case of RTPMMA), thus much lower levels of thermal stresses are built.

3.2 Damage initiation

As already mentioned it was assumed that damages consisted of crazes initiated in the matrix near the rubbery particles. It is usually admitted that crazes occur in HIPS, shear bands in RTPMMA and a mixture of both in ABS [1, 2, 6]. However, in experiments conducted on materials containing very low volume fractions of particles, secondary crazes were observed in PMMA [25] and shear bands in HIPS [26]: probably both kinds of damages always exist in damaged zones at crack tips, and only the ratio between them varies.

Breuer [27] reviewed the craze initiation criteria in multiaxial stress fields. The main source of errors when deriving such criteria lies in the premature surface crazing; valid crazing criteria (and shear yielding criteria as well) can be represented in the space of positive principal stresses by a critical surface resembling a portion of sphere or, better, a paraboloid with the axis of symmetry [1, 1, 1]. They are thus two-parameter criteria (time and temperature dependences excepted).

The criterion established by Argon and Hannoosh [28] has been used in this work; in the case of the PS matrix the parameters published in reference [13] have been used. For PMMA, the parameters for Argon's criterion have been calculated using data published by Sternstein *et al.* [29, 30] and Kawagoe [31] (the equivalence of different criteria occurring in uniaxial tension [27]. Transposition of the data obtained at the rather high temperatures (45 to 75° C) used by these authors to room temperature has been undertaken by means of Williams, Landell and Ferry's formalism; it has been simply checked that the calculated values correctly predicted the bulk craze initiation stress in uniaxial tension.

The criterion is expressed as a function of the mean shear stress ("Mises equivalent stress") σ_e and the negative pressure σ_p, which are defined as follows [12]:

$$\sigma_e = \left[\sum_{i<j}\sum (\sigma_i - \sigma_j)^2/2\right]^{1/2} = [I_1^2 + 3I_2]^{1/2} \quad (10)$$

$$\sigma_p = \sum_i \sigma_i/3 = I_1/3 \quad (11)$$

(where the σ_i are the principal stresses and I_1, I_2 are the two first invariants of the stress tensor). In the case where σ_e is constant, the criterion can be written:

$$\sigma_p + U_1 > U_2/\sigma_e \quad (12)$$

where U_1 and U_2 are material parameters. The time dependence is included in U_1; for polystyrene at 25° C the parameters are:

$$U_2 = 725\,\text{MPa}^2 \qquad U_1 = 10.3 + 0.62 \log (t)$$

(U_1 in MPa) (13)

where t (in seconds) is the time during which σ_e is applied; the time dependence of σ^* is weak and for the calculations presented here a value of $U_1 = 10.3$ MPa was used.

For PMMA at the same temperature (25° C):

$$U_2 = 3200\,\text{MPa}^2 \qquad U_1 \simeq 13.8\,\text{MPa}$$

(for t = 600 to 1200 sec) (14)

and at 20° C:

$$U_2 = 5670\,\text{MPa}^2 \qquad U_1 \simeq 14.6\,\text{MPa} \quad (15)$$

The corresponding craze initiation stresses in uniaxial tension are 30 MPa for PS at 25° C; 80 MPa at 25° C and 110 MPa at 20° C for PMMA. These values are in agreement with the craze surface stresses in these materials.

3.3. Results and discussion

The profile $r(\theta)$ of the damaged zone is the solution of a polynomial equation of the second degree (if thermal strinkage stresses are neglected); h is the largest projection of $r(\theta)$ on the y-axis of Fig. 1, and σ^* is obtained using h and Equation 3. The comparison of the experimental values of σ^* with the theoretical ones (see Table II) generally shows a reasonable agreement, except for some of the HIPS (S2, S4 and S5). For these materials that were not transparent enough it was not possible to obtain accurate experimental values of σ^* (the diffusion of light by the particles reduces the apparent size of the damaged zone, giving too high measured values of σ^*). In the other cases the experimental error is between 5 and 8%; the remaining discrepancies can be explained by differences in rubber to rigid ratio and in rubber modulus between real and model particles.

For PMMA it may seem surprising to find an agreement with a model that assumes that the crack-tip

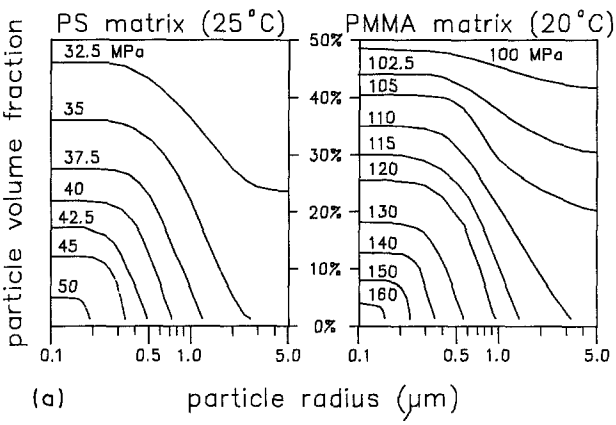

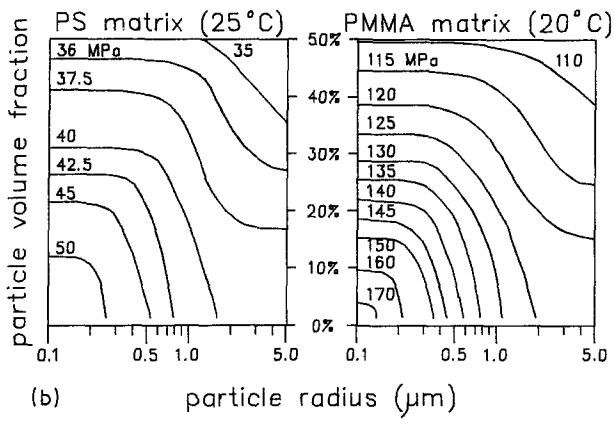

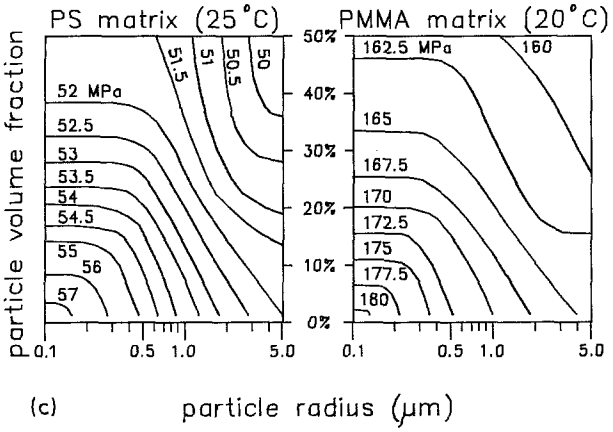

Figure 9 Theoretical values of the characteristic stress σ^* defined by Equation 3, in the case of (a) CS/R particles in PS matrix at 25° C and in PMMA matrix at 20° C. Lines of equal σ^* are plotted against two parameters, the number average particle radius (r_p in μm, x-axis) and the particle volume fraction (v_p in %, y-axis). (b) Same as (a) for CS/H particles; (c) Same as (a) for MI particles.

damaged zone consists of crazes; however two explanations can be proposed. Both are connected with the particular character of the crack-tip stress field, which has its three principal stresses positive: (1) in such a stress field with a negative pressure component the probability of craze initiation is increased as against that of shear band initiation [6], thus the assumption may be right; (2) even if the assumption is wrong and the damaged zone mainly consists of shear bands, the corresponding initiation stress is very close to the one of crazes in these conditions [27], thus an apparent agreement may occur.

The influence of the various parameters does not appear clearly in the analytical expressions of $r(\theta)$ and σ^*, so it has been illustrated in Fig. 9 where σ^* has been plotted as a function of two variables, namely the number average particle radius r_p and the particle volume fraction v_p, for the three particle morphologies considered in this paper. The lines of equal σ^* look like sigmoids. For a given matrix σ^* can be decreased by choosing more compliant particles, or by increasing the size and volume fraction of the particles. An increase in r_p is more efficient at moderate particle volume fractions (around 20%) than at higher ones. In PS containing MI particles with diameters below 0.8 μm, a particle volume fraction of 40% is necessary for restoring the same value of σ^* as with 20% of 3 μm diameter particles. For particle diameters below 0.3 to 0.6 μm, σ^* is independent of the particle size.

It can also be seen on Figs 9a, b, c that σ^* can be decreased by increasing r_p even when $v_p \simeq 0$; this is consistent with the fact that σ^* is a parameter that reflects the local initiation of damages in a heterogeneous material, but does not characterize completely the fracture toughness. At very low particle volume fractions, materials differing only by the size of the particles they contain may have very different σ^*, but almost similar K_{IC} or G_{IC}.

The time and temperature dependences have not been reported here; it would be interesting to study them comparatively for the cases of craze and shear band initiation, since both mechanisms do not dissipate the same amount of energy. In this regard the method presented here, which yields the theoretical envelope $r(\theta)$ of the zone where energy dissipation occurs (thus its volume too), may offer a new approach to the problem of crack propagation and blunting in tough polymers. Other applications concern the prediction of the onset of unstable crack growth, which seems to follow a critical damaged zone size criterion [32], and the theoretical calculation of critical values of the stress intensity factor at the onset of crack propagation (K_{Ic}) or during stable crack growth (K_{Ip}).

Other mechanisms of damage formation could be modelled in a similar manner, for example two-step mechanisms where particle debonding or cavitation relieves the negative pressure and promotes shear band initiation. The main difference expected in the case of shear bands would be a much lower dependance on particle size.

Acknowledgements

The work reported here was financed by the French Ministère de la Recherche et de la Technologie (grant Nr. 86A0535), and by the company NORSOLOR (grant Nr. 86/22). The authors also wish to thank Professor C. B. Bucknall and Dr I. K. Partridge who supplied some of the materials used in this study (see Table I and [21]).

References

1. A. J. KINLOCH and R. J. YOUNG, "Fracture Behaviour of Polymers" (Applied Science Publishers, London, 1983) Ch. 11.
2. C. B. BUCKNALL, "Toughened Plastics" (Applied Science Publishers, London, 1977).
3. F. HAFF, H. BREUER and J. STABENOW, *J. Macromol. Sci. – Phys.* **B14** (1977) 387.
4. H. KESKKULA, M. SCHWARZ and D. R. PAUL, *Polymer* **27** (1986) 211.
5. A. M. DONALD and E. J. KRAMER, *J. Appl. Polym. Sci.* **27** (1982) 3729.
6. C. B. BUCKNALL and A. MARCHETTI, *Polym. Eng. Sci.* **24** (1984) 535.
7. J. BOTSIS, A. CHUDNOVSKY and A. MOET, *Inter. J. Fracture* **33** (1987) 263.
8. *Idem, ibid.* **33** (1987) 277.
9. J. G. WILLIAMS, European Group on Fracture, private communication (1988).
10. K. NIKPUR and J. G. WILLIAMS, *J. Mater. Sci.* **14** (1979) 467.
11. J. R. RICE, *ASME Trans., J. Appl. Mech.* (1968) 379.
12. M. E. BOYCE, S.M. Thesis, MIT (1983).
13. M. E. BOYCE, A. S. ARGON and D. M. PARKS, *Polymer* **28** (1987) 1680.
14. R. J. OXBOROUGH and P. B. BOWDEN, *Phil. Mag.* **30** (1974) 171.
15. T. RICCO, A. PAVAN and F. DANUSSO, *Polymer* **20** (1979) 367.
16. L. J. BROUTMAN and G. PANIZZA, *Int. J. Polym. Mater.* **1** (1971) 95.
17. M. MATSUO, T. WANG and T. K. KWEI, *J. Polym. Sci.* **A2** (1972) 1085.
18. F. J. GUILD and R. J. YOUNG, *J. Mater. Sci.* **24** (1989) 298.
19. P. TRASSAERT and R. SCHIRRER, *ibid.* **18** (1983) 3004.
20. D. BROEK, in "Elementary Engineering Fracture Mechanics" (Sijthoff and Noordhoff Publishers, Alphen aan den Rijn, The Netherlands, 1978) Ch. 4.
21. C. B. BUCKNALL, P. DAVIES and I. K. PARTRIDGE, *J. Mater. Sci.* **22** (1987) 1341.
22. J. N. GOODIER, *ASME Trans.* **55** (1933) 39.
23. O. ISHAI and L. J. COHEN, *J. Compos. Mater.* **2** (1968) 302.
24. P. C. PARIS and G. C. SIH, *ASTM Spec. Techn. Publ.* **381** (1965) 30.
25. O. MAUZAC and R. SCHIRRER, *J. Appl. Polym. Sci.* **38** (1989) 2289.
26. *Idem*, unpublished results.
27. H. BREUER, *NATO ASI Ser.* **89** (1985) 375.
28. A. S. ARGON and J. G. HANNOOSH, *Phil. Mag.* **36** (1977) 1195.
29. S. S. STERNSTEIN and F. A. MYERS, *J. Macromol. Sci. – Phys.* **B8** (1973) 539.
30. S. S. STERNSTEIN and L. ONGCHIN, *Polym. Preprints* **10** (1969) 1117.
31. M. KAWAGOE, *J. Polym Sci. – Phys.* **19** (1981) 1423.
32. I. NARISAWA and M. T. TAKEMORI, *Polym. Eng. Sci.* **28** (1988) 1462.

Received 13 July
and accepted 12 December 1989